Waterjet Self-Propulsion Simulation: A Body-Force Approach for Modelling the Pump

The 11th Symposium on High Speed Marine Vehicles
Naples, 25 & 26 October 2017

Waterjet Self-Propulsion Simulation: A Body-Force Approach for Modelling the Pump

A. Eslamdoost

Department of Mechanics and Maritime Sciences, Chalmers University of Technology, Gothenburg, Sweden

M. Hyensjö

Rolls-Royce Hydrodynamic Research Centre, Kristinehamn, Sweden

ABSTRACT: The waterjet pump can be treated in different ways in a Reynolds Averaged Navier-Stokes based numerical simulation. The most accurate model is to resolve the complete pump geometry with rotating impeller (e.g. rigid body rotation). Alternatively, in order to reduce the computational cost, a frozen rotor approach or a body-force model can be employed. In this paper, different body-force models are utilized to simulate the waterjet pump in self-propulsion. Then the body-force models are evaluated through a quantitative comparison of the pump flow rate, head rise and the detailed flow at the nozzle exit with the results obtained from the more sophisticated rigid body rotation and frozen rotor techniques. This evaluation reveals that a body-force model for pump induces very similar effects on the flow in comparison to the more sophisticated methods and can reliably be used for modelling waterjet-hull interaction effects in self-propulsion.

1 INSTRUCTIONS

According to the proposed procedure by The ITTC Specialist Committee on Validation of Waterjet the thrust of a waterjet unit is expressed based on the axial momentum flux change (gross thrust) through the control volume of the waterjet system shown in Figure 1(ITTC 24 2005). Surface 1 and surface 8 are the only surfaces of the control volume that the flow can pass through. Surface 2 is an imaginary surface, which separates the flow drawn into the ducting system from the rest of the flow field and no flow crosses this surface. All the other surfaces of the control volume are material boundaries and the flow cannot pass through. Surface 8 is the nozzle exit and Surface 1 is named the capture area and is located far enough in front of the intake ramp tangency point before inlet losses occur. As a practical solution, The ITTC Specialist Committee on Validation of Waterjet Test Procedure recommends one inlet length forward of the ramp tangency point (ITTC 24 2005).

The gross thrust of the waterjet is defined as,

$$T_g = \iint_{A_1+A_8} \rho u_x (u_k n_k) dA\,, \qquad k = x, y, z \quad (1)$$

where ρ is the water density, u is the velocity vector and n is the unit normal vector which points out of the control volume (van Terwisga 1996).

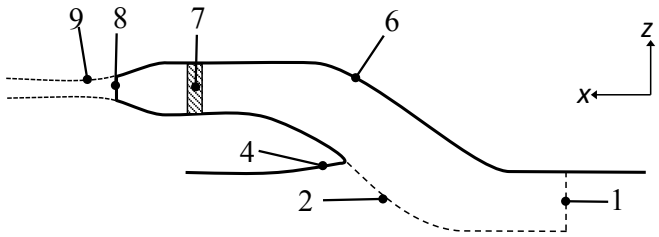

Figure 1. Section cut through the waterjet ducting system

By introducing a coefficient that takes the velocity-squared non-uniformity into account, Equation (1) can be re-written as follows,

$$T_g = \rho Q (c_{m8} \bar{u}_{8_x} - c_{m1} \bar{u}_{1x}), \qquad (2)$$

where, Q is the volumetric flow rate through the nozzle. $\bar{u}_{1x}$ and $\bar{u}_{8x}$ are the mean axial velocity through the capture area and the nozzle discharge section, respectively. The correction coefficient c_m is defined as follows,

$$c_m = \frac{1}{A_x}\iint_{A_x}\left(\frac{u_x}{\overline{u}_x}\right)^2 dA_x. \qquad (3)$$

A sensitivity analysis based on Equation (2) shows that an error of 1% in flow rate results in an error about 2.4-3.5% in gross thrust (van Terwisga 1996). This highlights the importance of the flow rate measurement.

An important part of a Reynolds Averaged Navier-Stokes (RANS) based numerical method for modelling the waterjet-hull interaction analysis is the pump modelling technique. There are two main techniques for the numerical simulation of the pump in waterjet self-propulsion using RANS; either modelling the actual pump geometry (i.e. Yang et al. (2014)) or employing a Body-Force Model (BFM) which does not resolve the detailed pump geometry elements such as impeller and guide vanes (see for instance Giles et al. (2010), Takai et al. (2011), Delaney (2011) and Eslamdoost et al. (2016)). In the latter approach, the flow head increases through a momentum source term (body-force) in the Navier-Stokes equations. Obviously, the full simulation of the pump flow provides more detailed information of the flow inside the pump, however it is rather costly in terms of computational power needed to perform such a simulation. In contrast, a body-force model fails to predict the actual flow inside the pump but comes with a less computational cost.

The objective of this paper is to compare the full pump geometry simulation with the alternative body-force approach employing a RANS solver. To this end, first, two well established methods of Moving Reference Frame (MRF) and Rigid Body Rotation (RBM) are used for modelling the actual pump geometry. Besides, three different body-force models are employed. In the first body-force model, the pump flow is only accelerated in the axial direction. In the second model, in order to take the pump swirl into account, the flow is accelerated not only in the axial direction but also in the tangential direction. Finally, a third body-force model is also studied. In this body-force model, opposite to the first and the second body-force models, the stator geometry is resolved and the impeller is modelled by an axial and tangential body-force distribution. The resultant flow rate and the head rise as well as the detailed flow at the nozzle discharge will be compared between the addressed models.

2 HULL AND WATERJET GEOMETRIES

The hull geometry used in this study is a test case designed at SSPA. The hull is 2.3 m long equipped with a stock mixed-flow waterjet pump and an intake designed by Roll-Royce. The pump inlet dimeter, D_i, is 90 mm and has 6 impeller blades and 12 guide vanes (Brown 2013). The hull geometry, the positioning of the waterjet unit as well as the pump geometry are shown in Figure 1.

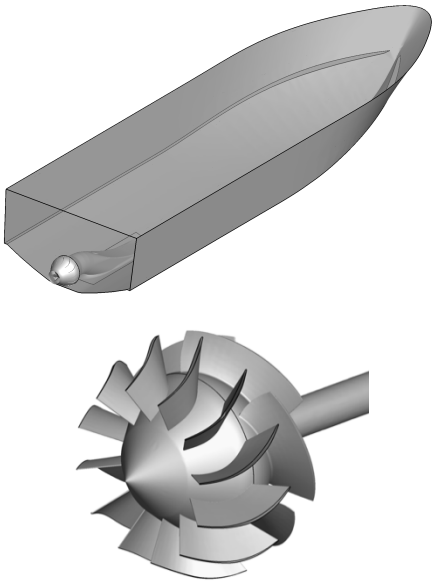

Figure 1: Hull and pump geometries.

3 METHOD

The numerical models and the computational grid which are used to carry out a set of self-propulsion simulations are presented in this section. The body-force models are also addressed.

3.1 Numerical models

The numerical simulations are carried out with the code STAR-CCM+ 12.02. A Finite Volume method is used to solve the steady-state and transient mass and momentum conservation equations in integral form. An implicit unsteady time stepping method is used in the code meaning that the method calculates the solution by solving an equation involving both the current time step solution and the latter one. This method has a wider stability range (Courant number larger than 1) and therefore allows large local time step. Turbulence is modelled using the SST $k-\omega$ model along with a wall treatment which switches between resolving the boundary layer down to the wall and a wall-function depending on the local y^+. The convection terms of the aforementioned transport equations are solved using the upwind second order discretization scheme and first order temporal discretization is used for the time stepping. Moreover, in order to capture the free-surface, the Volume of Fluid (VOF) method is employed. Convective terms in this equation are discretized using the HRIC-scheme (Muzaferija & Perić 1999). The free-surface interface is expected to be sharp since this equation resolves the free-surface within typically one cell. Details on discretization and solution methods can be

found in Ferziger and Perić (2003), Demirdžić and Muzaferija (1995) and Weiss et al. (1999).

The investigations in this study are carried out in self-propulsion meaning that the resultant of the waterjet thrust and the resistance cancel out each other. As already mentioned in the introduction section, the pump is modelled using MRF, RBM as well as three body-force models. The pump revolution rate is adjusted in order to obtain a zero net-force over the hull and waterjet system when the MRF and RBM techniques are used. The body-force approach and its different arrangements are addressed in Section 3.3.

3.2 Computational domain and grid generation

The computational domain, its extents and an overall presentation of the mesh distribution inside the domain are shown in Figure 2. Trimmed hexahedral grids with a set of refined regions are used around the hull. Trimmed grids allow anisotropic local refinement. The refinements are employed around the free-surface, the jet and the waterjet intake region to provide a better resolution of the results (Figure 3). Since the pump geometry is more sophisticated than the rather smooth geometry of the hull, polyhedral cells are employed inside the pump for a better representation of the curved surface of the impeller blades and guide vanes (Figure 4). Prism layers along walls are used to resolve the boundary layer. The average y^+ value on the hull and the duct is around 40 and around 5 on the surfaces inside the pump.

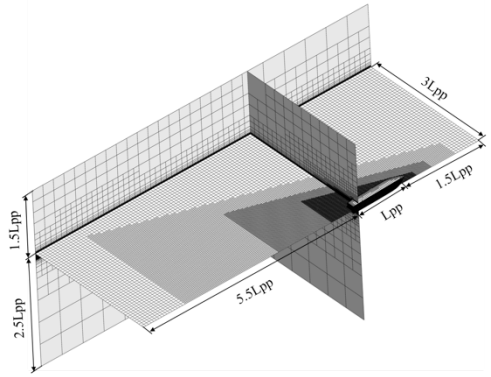

Figure 2: The structure of the mesh illustrating the refined zones. Arrows show the extent of the computational domain expressed in the hull Lpp.

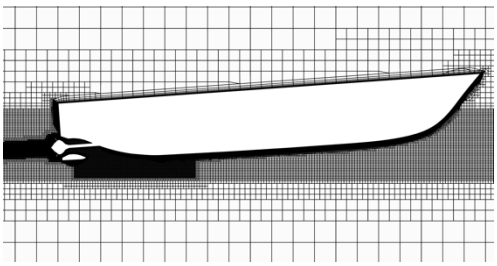

Figure 3: Mesh distribution on the symmetry plane.

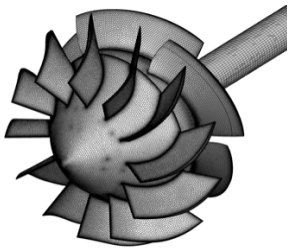

Figure 4: Polyhedral surface mesh inside the pump.

3.3 Body-force models

Three different body-force implementations for modelling the pump are discussed in this section. In the first model (BFM1), the impeller and guide vane blades are removed and only an axial body-force model is employed to represent the pump. The axial body-force is distributed uniformly inside the volume which encloses the impeller. The magnitude of the axial body-force is set to the resistance of the hull and ducting channel, including the shaft and the hub. The axial body-force per unit volume, B_a, reads as follows:

$$B_a = \frac{R_T}{\nabla_B}, \tag{4}$$

where R_T is the accumulated resistance of the waterjet-hull system and ∇_B is the volume of the region which the body-force is acting on.

In the second model the pump swirl is modelled through superimposing a tangential body-force component onto the axial component (BFM2). Generally, the guide vanes are designed to remove the swirl of the flow caused by the impeller. Therefore, for a swirl free pump, the torque exerted on the guide vanes will be as large as the impeller torque but in the opposite direction. According to this concept, the magnitude of the tangential body-force component is set to the accumulated torque of the impeller blades and the guide vanes. The tangential body-force component is applied to the same region as employed for the axial body-force component. It is a tricky task to find a proper body-force distribution which eventually results in the same swirl distribution as in the actual flow. In this study, instead of a uniform tangential body-force distribution, a uniform induced torque is suggested. Thus, the tangential body-force needs to be a function of radial distance from the shaft line. The tangential body-force per unit volume, B_t, reads as follows:

$$B_t = \frac{\tau \times \frac{1}{r}}{\nabla_B}, \tag{5}$$

where τ is the pump accumulated torque and r is the radial distance from the shaft center line. The torque in this model is obtained from the Sliding Mesh simulations.

In the third model (BFM3), the guide vanes are present in simulations and just the impeller blades are removed. The implementation of this body-force model is similar to BFM2 but the employed thrust and torque are different. The resistance of the guide vanes also has to be considered in the accumulated resistance of the system when the axial body-force is distribution is computed in equation (4). Since it is just the impeller geometry which is missing in this model, only the impeller's torque is used in equation (5). The modified pump geometries which are used with the aforementioned body-force models are presented in Figure 5.

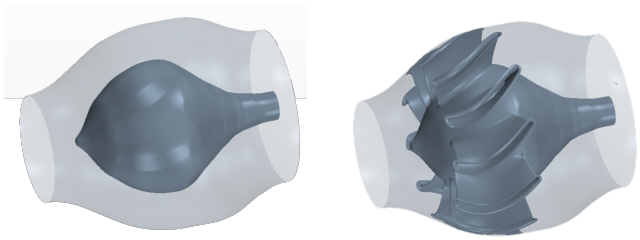

Figure 5: Geometries used with different body-force models. BFM1 and BFM2 (left) BFM3 (right).

4 RESULTS AND DISCUSSIONS

A set of self-propulsion simulations were carried out at Froude number 0.5 and 1.0 with all the pump models introduced in Section 3. An overview of the free-surface pattern around the hull and the jet profile in self-propulsion simulation is presented in Figure 6.

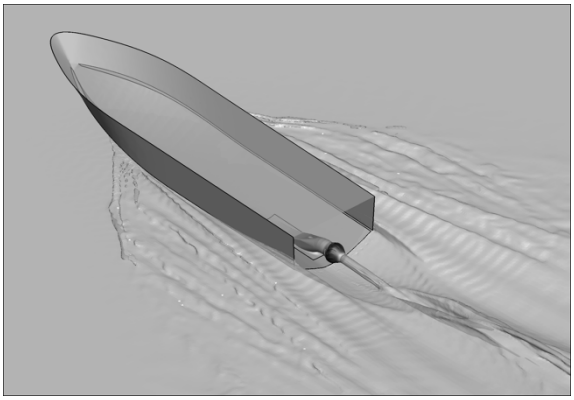

Figure 6: A generic representation of the free-surface around the hull and the discharged jet at Froude number 1.0.

As indicated earlier the tangential body-force component is obtained from the results of the full pump simulation using RBM. The impeller torque and the guide vanes' torque at Froude number 0.5 and 1.0 are plotted in Figure 7 and Figure 8, respectively. The horizontal axis in these figures shows the guide vane passage number. As shown in Figure 1, the pump used in this study has 12 guide vanes and thus during one full revolution of the pump each impeller blade encounters 12 guide vane passages. This is the reason for seeing 12 transient peaks in the computed torque of the guide vanes in Figure 7 and Figure 8. The oscillations in the computed torques are correlated to the relative position of the impeller blades and the guide vanes. The minimum torque occurs when the trailing edge of the impeller blades meet the guide vane leading edge. On the other hand, the maximum transient torque of both the impeller and the stator occurs when the impeller blade trailing edges is located half way through one of the guide vanes passage.

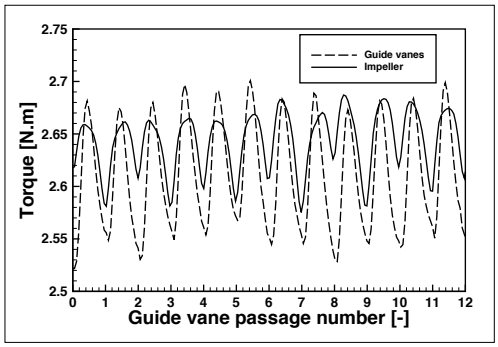

Figure 7: Impeller and guide vanes torques at Froude number 0.5. Note that these torques act in opposite directions.

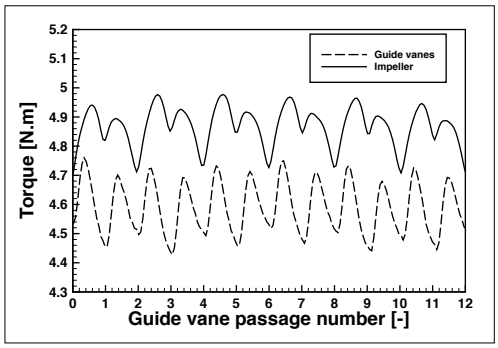

Figure 8: Impeller and guide vanes torques at Froude number 1.0. Note that these torques act in opposite directions.

Note that the impeller and the guide vanes torques which are depicted in Figure 7 and Figure 8 act in opposite directions. Ideally, the counteracting stator torque should be as large the impeller torque to cancel out the swirl in the flow induced by the impeller. This almost happen at Froude number 0.5 but not at Froude number 1.0. An imbalance exists between the impeller torque and the stator torque at Froude number 1.0. The time averaged torques acting on the impeller and the stator (mean value of the curves depicted in Figure 7 and Figure 8) are inserted to Equation (5) for the calculation of the tangential body-force component.

The pump mass flow rate, $\dot{m}$, and the head increase through the pump, Δh, is used to quantify the difference between all the body-force models and the MRF and RBM results. This data is presented in Table 1 and Table 2 for Froude number 0.5 and 1.0, respectively. In order to calculate the head rise, the

surface averaged values of the velocity magnitude and pressure are obtained at a section just before the pump (subscript 1) as well as the nozzle exit section (subscript 2). We have used the results of RBM simulation as a reference and the deviation of the results from that of RBM are called error in these two tables.

The comparison of the mass flow rate computed from different approaches at both of the Froude numbers reveals a minute deviation from the result of the RBM technique. The maximum deviation is less than 0.3%. Which can result in about 1% deviation in gross thrust calculation, according to the sensitivity analysis performed by van Terwisga (1996).

The average velocities on section 1 and section 2 (just before and after the pump) are almost the same for different approaches however the computed mean pressure differs slightly when the results of the investigated models are compared. Despite the weak contribution of the pressure term to the head increase between section 1 and section 2, the difference between the average pressures obtained from the various pump models is the main reason for the deviation of the head rise from that of the RBM. The head rise deviation is the largest for BFM1 at both of the studied Froude numbers. The deviation decreases by introduction of the pump induced swirl into the body-force models (BF2 and BF3).

Table 1. The flow rate and the head increase through the pump at Froude number 0.5 for different pump models.

	$\dot{m}$	$\dot{m}$ error	P_1	P_2	V_1	V_2	Δh	Δh error
	[kg/s]	[%]	[Pa]	[Pa]	[m/s]	[m/s]	[m]	[%]
BF1	16.30	0.12	-535	2537	2.46	6.57	2.21	1.81
BF2	16.32	0.25	-545	2445	2.46	6.58	2.20	1.64
BF3	16.32	0.25	-615	2267	2.46	6.58	2.19	1.13
MRF	16.33	0.31	-519	2234	2.46	6.58	2.18	0.63
RBM	16.28	-	-520	2213	2.45	6.56	2.17	-

Table 2. The flow rate and the head increase through the pump at Froude number 1.0 for different pump models.

	$\dot{m}$	$\dot{m}$ error	P_1	P_2	V_1	V_2	Δh	Δh error
	[kg/s]	[%]	[Pa]	[Pa]	[m/s]	[m/s]	[m]	[%]
BF1	22.30	-0.27	2732	4576	3.36	8.99	3.73	1.00
BF2	22.40	0.18	2685	4134	3.37	9.03	3.73	0.77
BF3	22.34	-0.09	2823	4165	3.37	9.01	3.70	-0.04
MRF	22.32	-0.18	2862	4029	3.36	9.00	3.67	-0.70
RBM	22.36	-	2829	4124	3.37	9.02	3.70	-

Evaluation of the addressed pump models can also be carried out through the comparison the detail flow at the nozzle exit section. The pressure and the swirl distribution at the nozzle exit are shown in Figure 9 for this purpose. The swirl is defined as the magnitude of non-axial velocity components to the axial velocity.

Studying the contours presented in Figure 9, one can realize the existence of a hub vortex in all models except than BFM1. The larger swirl in the centre of the nozzle exit section and simultaneously the low-pressure area at the same region is the effect of the hub vortex. In the models which consider the pump swirl, the minimum pressure is predicted in the centre, where the hub vortex is located. Among the models, BFM3 and MRF provide a closer match of the nozzle exit pressure distribution with the RBM result. However, the hub vortex strength is under-predicted in both of the models.

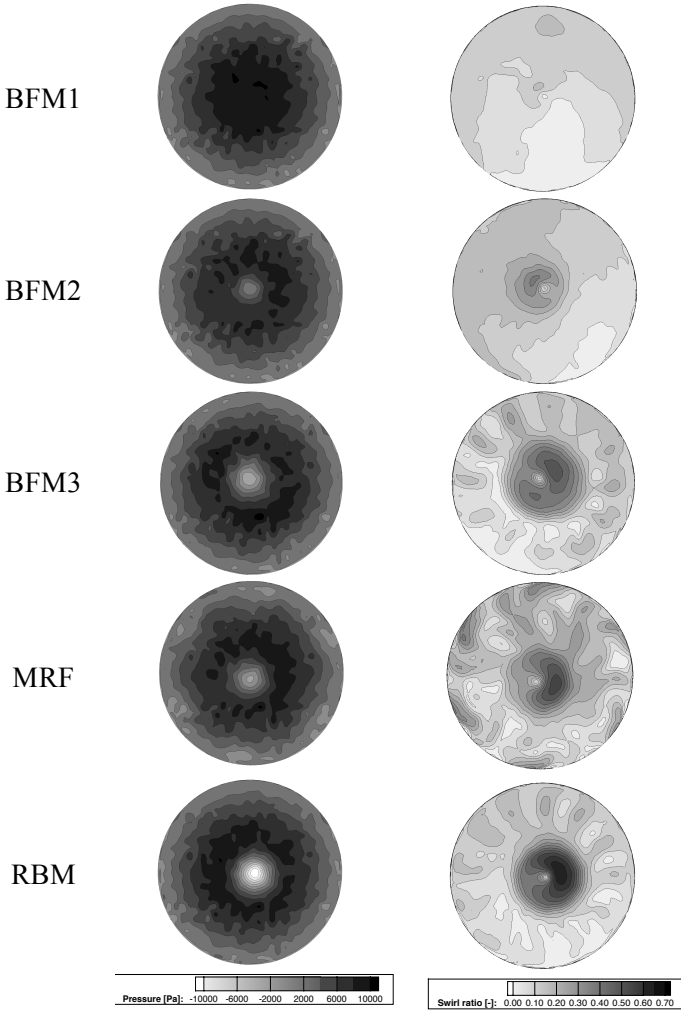

Figure 9: Pressure (left) and swirl (right) distribution at the nozzle exit section obtained from different models.

The swirl contour plots show a more uniform flow with less disturbance at the nozzle exit for BFM1 and BFM2 in comparison to the other models. The reason is the absence of the stator geometry in these pump treatment approaches. The lower part of the nozzle exit section has less swirl in comparison to the upper half. The reason is the inflow wake ahead of the pump. As seen in Figure 10, the lower half of the inflow to the pump has larger axial velocity rather than its upper half. A recirculation region on the upper part of the ducting channel as well as the impeller shaft, which acts as a hinder, slow down the flow on the upper part. Thus, the flow at the upper side of the pump inlet has a lower momentum and is more prone to change direction through the pump (larger swirl).

Except the hub vortex region in BFM2, the swirl distribution has similar pattern as in BFM1 but rotated in the direction of the tangential body-force around the centre axis. The tangential component of the body-force which has been applied in the form of a uniform torque distribution to the region surrounding the impeller (see Equation (5)) results in an almost rigid body rotation of the flow passing through this region. Of course, this is not completely true since the radial distance between the pump housing and the hub changes across the region which the body-force is applied. The flow particles may experience different accumulated tangential (as well as axial) body-force based on the path which they travel through the aforementioned region. The assumption of pure solid body rotation of the flow inside the body-force region is not precise but can explain the dislocation of the low swirl region in the lower part of the nozzle exit in BF1 to a new position in BFM2.

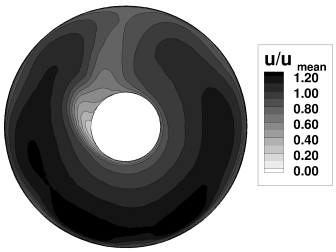

Figure 10: Non-dimensional axial velocity ratio.

The stator is present in the rest of the pump treatment models and thus the wake of the guide vanes is detectable at the nozzle exit (Figure 9). The flow computed by BF3 matches well with the result of RBM, however the MRF technique results predict a set of non-coherent flow structures at the nozzle exit which do not match with the RBM results.

5 CONCLUSIONS

Three body-force models are used for modelling the waterjet pump. The first model accelerates the flow only in the axial direction but the other two consider the tangential acceleration of the flow due to the action of the pump. In the two first models the impeller blades and guide vanes are removed from the model whereas in the third model the guide vanes are kept in place. The body-force components are uniformly distributed inside the region which surrounds the impeller. In order to reach the self-propulsion point, the axial body-force component iteratively is set to be equal to the waterjet-hull system's resistance. The tangential body-force component depends on the pump design and its operating condition and should be known before the application of the body-force models with the tangential components (BF2 and BF3). In this study, the tangential body-force components (function of impeller and guide vanes torque) are obtained from a full pump simulation using a rigid body rotation model for simulating the impeller rotation. This information can also be acquired from measurement.

Due to the large dependence of the waterjet gross thrust on the pump flow rate, one important objective of using different body-force models was to investigate the sensitivity of the pump flow rate obtained through these models in comparison to the more sophisticated rigid body rotation technique. It was revealed that the flow rate discrepancy for all of the employed body-force models are below 0.3% in comparison to the flow rate computed from the time dependent rigid body rotation approach. This finding indicates that including or excluding the tangential body-force component does not play an important role on the computed flow rate. However, the application of the tangential body-force component has a clear effect on the computed pump head rise. The best head rise match was achieved with the third body-force model which was comprised of the tangential body-force component as well as the guide vanes. Moreover, in this model, the flow structures at the nozzle exit are resolved quite well in comparison to the rigid body rotation technique results.

This study also shows that the mass flow rate and head rise computed from the steady state moving reference frame technique are very close to the ones computed from the transient rigid body rotation approach. However, the flow structures are the nozzle exit are not resolved well.

According to the aforementioned remarks, one may prioritize the application of any of the discussed techniques in waterjet self-propulsion simulation. In case the computation cost and time are not limiting constrains (which usually is not the case), the rigid body rotation technique could be employed; otherwise, any of the steady state moving reference frame or body-force models could be employed. The third body-force model results are quite reliable but one should bear in mind that the impeller torque needs to be known prior to the simulation. The moving reference frame technique does not need this information but as a drawback fails to predict the flow structures at the nozzle exit accurately. The body-force model requires less computational cost in comparison to the moving reference frame since there is no need to include the impeller blades and mesh the full impeller geometry in this model.

REFERENCES

Brown, M., 2013. *Model tests of a complete waterjet-hull system. In SSPA report RE40084817-16-00-B.*

Delaney, K.P., 2011. *Use of RANS for Waterjet Analysis of a*

High-Speed Sealift Concept Vessel. In International Conference on Computational Methods in Marine Engineering (MARINE).
Demirdžić, I. & Muzaferija, S., 1995. *Numerical method for coupled fluid flow, heat transfer and stress analysis using unstructured moving meshes with cells of arbitrary topology. Computer Methods in Applied Mechanics and Engineering, 125, pp.235–255*.
Eslamdoost, A., Larsson, L. & Bensow, R., 2016. *Net and gross thrust in waterjet propulsion. Journal of Ship Research, 60(2)*.
Ferziger, J.H. & Perić, M., 2003. *Computational Methods for Fluid Dynamics Springer, ed. Physics Today*.
Giles, W. et al., 2010. *The Advanced WaterJet: Propulsor Performance and Effect on Ship Design. In International Naval Engineering Conference (INEC). Portsmouth, UK*.
ITTC 24, 2005. *The Specialist Committee on Validation of Waterjet Test Procedures, Final Report and Recommendations to the 24th ITTC*.
Muzaferija, S. & Perić, M., 1999. *Computation of free surface flows using interface-tracking and interface- capturing methods. In Nonlinear Water Wave Interaction. Southampton: WIT Press, pp. 59–100.*
Takai, T., Kandasamy, M. & Stern, F., 2011. *Verification and validation study of URANS simulations for an axial waterjet propelled large high-speed ship. Journal of Marine Science and Technology, 16(4), pp.434–447.*
van Terwisga, T., 1996. *Waterjet-Hull Interaction. PhD Thesis, Delft Technical University.*
Weiss, J.M., Maruszewski, J.P. & Smith, W.A., 1999. *Implicit solution of preconditioned Navier-Stokes equations using algebraic multigrid. AIAA, 37, pp.29–36*.
Yang, Q., Wang, Y. & Zhang, Z., 2014. *Numerical prediction of the fluctuating noise source of waterjet in full scale. Journal of Marine Science and Technology, 19(4), pp.510–527.*